Molecular Cell
Article

PHD Finger Recognition of Unmodified Histone H3R2 Links UHRF1 to Regulation of Euchromatic Gene Expression

Eerappa Rajakumara,[2,9] Zhentian Wang,[1,9] Honghui Ma,[1] Lulu Hu,[1] Hao Chen,[1] Yan Lin,[1] Rui Guo,[1] Feizhen Wu,[1] Haitao Li,[3] Fei Lan,[4] Yujiang Geno Shi,[1,5] Yanhui Xu,[1,6] Dinshaw J. Patel,[2,*] and Yang Shi[1,7,8,*]
[1]Laboratory of Epigenetics, Institute of Biomedical Sciences, Fudan University, Shanghai 200032, China
[2]Structural Biology Program, Memorial Sloan-Kettering Cancer Center, New York, NY 10065, USA
[3]Center for Structural Biology, School of Life Sciences and School of Medicine, Tsinghua University, Beijing 100084, China
[4]Constellation Pharmaceuticals, Cambridge, MA 02140, USA
[5]Endocrinology Division, Brigham and Women's Hospital, Harvard Medical School, Boston, MA 02115, USA
[6]State Key Laboratory of Genetic Engineering, School of Life Sciences, Fudan University, Shanghai 200433, China
[7]Department of Biochemistry, Fudan University Medical School, Shanghai 200032, China
[8]Division of Newborn Medicine and Program in Epigenetics, Department of Medicine, Children's Hospital, Harvard Medical School, Boston, MA 02115, USA
[9]These authors contributed equally to this work
*Correspondence: pateld@mskcc.org (D.J.P.), yshi@hms.harvard.edu (Y.S.)
DOI 10.1016/j.molcel.2011.07.006

SUMMARY

Histone methylation occurs on both lysine and arginine residues, and its dynamic regulation plays a critical role in chromatin biology. Here we identify the UHRF1 PHD finger (PHD_{UHRF1}), an important regulator of DNA CpG methylation, as a histone H3 unmodified arginine 2 (H3R2) recognition modality. This conclusion is based on binding studies and cocrystal structures of PHD_{UHRF1} bound to histone H3 peptides, where the guanidinium group of unmodified R2 forms an extensive intermolecular hydrogen bond network, with methylation of H3R2, but not H3K4 or H3K9, disrupting complex formation. We have identified direct target genes of UHRF1 from microarray and ChIP studies. Importantly, we show that UHRF1's ability to repress its direct target gene expression is dependent on PHD_{UHRF1} binding to unmodified H3R2, thereby demonstrating the functional importance of this recognition event and supporting the potential for crosstalk between histone arginine methylation and UHRF1 function.

INTRODUCTION

Chromatin covalent modifications, which include DNA methylation and histone posttranslational modifications, play an important role in epigenetic regulation. Histone N-terminal tails undergo extensive modifications including methylation on lysine (K) and arginine (R) residues. Methylation of different lysine residues of histone H3 and H4 is recognized by a variety of protein modalities, including the plant homeodomain (PHD), PWWP, and chromodomains (Taverna et al., 2007). Such recognition mechanisms confer elaborate regulatory functions in a plethora of chromatin template-based biological processes including gene regulation, DNA replication, and recombination. Recent studies further demonstrate that both methylated and unmethylated lysine residues are recognized by specific protein modalities important for regulation of gene expression (Lan et al., 2007; Ooi et al., 2007; Shi et al., 2006). In contrast, significantly less is known about how histone arginine residues are recognized, although arginine methylation plays equally important roles (Bedford and Clark, 2009).

Here we report the identification of the PHD finger domain in UHRF1 (PHD_{UHRF1}) as a histone H3 tail-binding module recognizing unmodified arginine residue 2 of histone H3 (H3R2). UHRF1 (ubiquitin-like, with PHD and RING finger domains 1) (also called NP95 and ICBP90) is required for the maintenance of CpG DNA methylation (Bostick et al., 2007; Sharif et al., 2007) and is composed of multiple protein modalities (Figure 1A), including SRA, which binds hemimethylated CpG (Bostick et al., 2007; Sharif et al., 2007), a Tudor domain that binds trimethylated histone H3 lysine 9 (H3K9me3) (Walker et al., 2008), as well as a PHD domain, whose histone binding partners remain unclear (Karagianni et al., 2008; Papait et al., 2008). UHRF1 is mainly localized to pericentromeric heterochromatin (PCH) (Papait et al., 2007), but recent studies suggest that UHRF1 also localizes to specific euchromatic regions, possibly playing a role in transcriptional repression (Daskalos et al., 2011; Kim et al., 2009). UHRF1 is believed to regulate PCH function as well as transcription of certain tumor suppressor genes (Daskalos et al., 2011). However, mechanisms underlying recruitment of UHRF1 to either heterochromatic or euchromatic regions remained largely unknown.

We show that in contrast to $Tudor_{UHRF1}$, which binds H3K9me3 (Walker et al., 2008), PHD_{UHRF1} specifically binds unmodified H3. Surprisingly, this binding is significantly reduced by H3R2 methylation but largely unaffected by H3K4 and H3K9 methylation, suggesting that PHD_{UHRF1} binds H3 via recognition

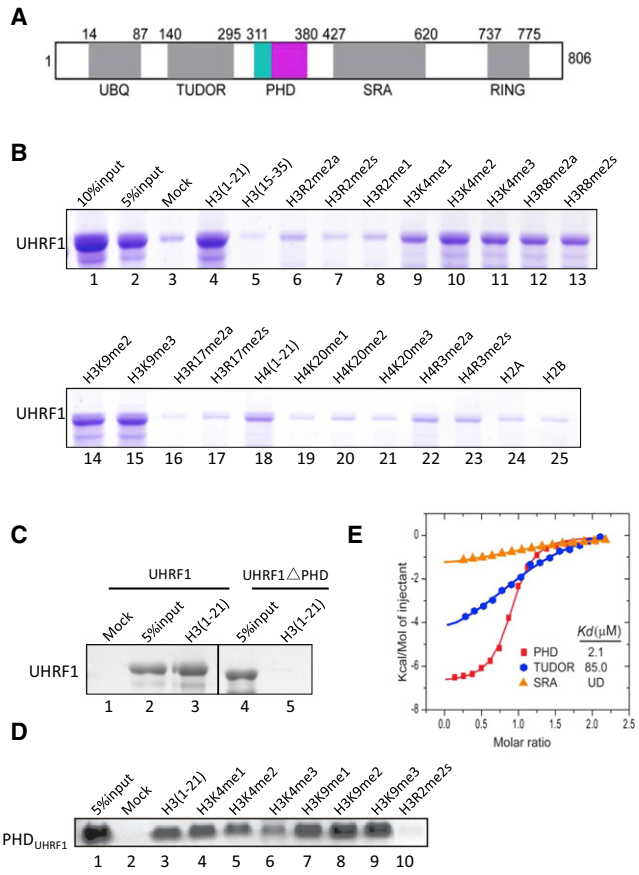

Figure 1. PHD$_{UHRF1}$ Recognizes Unmodified Histone H3 Tail

(A) Schematic representation of domain structure of human UHRF1. Numbers indicate amino acid positions at the boundaries of various domains.

(B–D) In vitro binding assays using various biotinylated histone peptides containing the indicated modifications. Either recombinant full-length UHRF1 or PHD$_{UHRF1}$ was incubated with biotinylated histone peptides immobilized onto streptavidin Sepharose beads. Bound proteins were subjected to SDS-PAGE and stained by Coomassie blue.

(E) ITC plots for binding of histone H3(1-10) to Tudor, PHD, and SRA domains of URHF1 with dissociation constant (Kd) values indicated. UD, undetectable.

of unmodified H3R2. This hypothesis is supported by the structure of PHD$_{UHRF1}$ in complex with H3 peptides, which identified H3R2 as a major contact site for PHD$_{UHRF1}$, together with the N-terminal amino group and side chain of the first alanine residue on H3, which likely helps anchor PHD$_{UHRF1}$ and therefore contributes to the unmodified R2 recognition specificity. Isothermal titration calorimetry (ITC) provided binding affinities of PHD$_{UHRF1}$ for either unmodified or modified H3 with methylation at R2, K4, and K9, reinforcing the notion that unmodified R2 is the major contact site for PHD$_{UHRF1}$. Genome-wide expression microarray analysis coupled with chromatin immunoprecipitation (ChIP) identified a number of UHRF1 direct target genes whose expression is repressed by UHRF1. Importantly, point mutations that disrupt PHD$_{UHRF1}$ binding to unmodified H3R2 also abrogated the ability of UHRF1 to repress target gene expression, while these mutations have no effect on UHRF1 PCH localization. Taken together, we have provided binding, structural, and functional data identifying PHD$_{UHRF1}$ as an unmodified H3R2 binder. Our findings suggest that recognition of the unmodified H3R2 by PHD$_{UHRF1}$ may represent an important mechanism for targeting UHRF1 to euchromatic regions and that histone H3R2 methylation may impact UHRF1 function by regulating its chromatin accessibility.

RESULTS

PHD$_{UHRF1}$ Recognizes Unmodified H3 Tail

As discussed above, UHRF1 is mainly localized to PCH, but it may also be present at euchromatic loci (Kim et al., 2009). Insight into how UHRF1 is recruited to these different regions of the genome is important for understanding mechanisms that underlie UHRF1-mediated biological processes. UHRF1 is composed of multiple protein modalities. In addition to the RING finger domain that mediates ubiquitylation (Citterio et al., 2004), it also contains Tudor, PHD, and SRA domains that mediate interactions of UHRF1 with histone and DNA, respectively (Bostick et al., 2007; Karagianni et al., 2008; Sharif et al., 2007; Walker et al., 2008) (Figure 1A). Previous studies suggested that PHD$_{UHRF1}$ binds H3K9me3 (Karagianni et al., 2008). However, one recent study showed that H3K9me3 binding is also mediated by Tudor$_{UHRF1}$ (Walker et al., 2008). Thus, exactly what PHD$_{UHRF1}$ binds remains unclear.

To address this issue, we first carried out in vitro binding assays using purified full-length UHRF1 and a collection of histone peptides with or without modifications. As shown in Figure 1B, UHRF1 specifically and robustly binds the unmodified, N-terminal histone H3 tail (aa 1–21) (lane 4), but not the more internal sequence of H3, either unmodified (aa 15–35, lane 5) or methylated on R17 (aa 15–35, lanes 16–17). UHRF1 also showed little or no binding to unmodified or methylated histone H4 (Figure 1B, lanes 18, 19–23), and to unmodified H2A or H2B (aa 1–21) (Figure 1B, lanes 24–25). Importantly, di- or trimethylation of H3K4 and H3K9, as well as H3R8 dimethylation, by and large did not significantly affect binding (Figure 1B, lanes 9–15). In contrast, methylation of H3R2 significantly reduced binding (Figure 1B, lanes 6–8), indicating that H3R2 may be a critical contact site for UHRF1. Deletion of the PHD domain from UHRF1 abrogated binding, suggesting that PHD$_{UHRF1}$ is necessary for UHRF1 to bind H3 (Figure 1C, compare lane 5 with lane 3). Finally, the PHD$_{UHRF1}$ domain alone was sufficient to bind unmodified H3, and binding was similarly impeded by methylation at H3R2 but largely unaffected by methylation at H3K9 (Figure 1D). ITC analysis determined the binding affinity (Kd) between PHD$_{UHRF1}$ and unmodified H3 to be approximately 2.1 μM (Figure 1E). In contrast, Tudor$_{UHRF1}$, which mainly recognizes H3K9me3 (Walker et al., 2008), had significantly less affinity for the unmodified H3 (Kd = 85.0 μM). Furthermore, the SRA$_{UHRF1}$ domain, which binds hemimethylated DNA, had no detectable binding to histone H3 (Figure 1E). Taken together, these findings suggest that among the various protein modalities present in UHRF1 (Figure 1A), PHD$_{UHRF1}$ is responsible, and is both necessary and sufficient for binding unmodified H3, possibly via recognition of the unmodified R2 residue.

Table 1. Crystallographic Data Collection and Refinement Statistics of PHD$_{UHRF1}$ in Free and Peptide-Bound States

Crystal	UHRF1 PHD-H3(1-9)	UHRF1 PHD-H3(1-9)K4me3	UHRF1 PHD Free State
Beamline	BNL X29	APS 24ID-C	Home source
Wavelength	1.2828	0.97918	
Space group	$P4_32_12$	$P4_32_12$	$I2_12_12_1$
Unit cell			
a, b, c (Å)	42.62, 46.62, 183.48	42.62, 46.62, 183.48	53.74, 53.81, 128.48
α, β, γ (°)	90, 90, 90	90, 90, 90	90, 90, 90
Resolution (Å)	20–1.80 (1.86–1.80)[a]	20.0–1.95 (2.02–1.95)[a]	20.0–2.65 (2.74–2.65)[a]
R_{sym}	0.069 (0.54)	0.12 (0.78)	0.064 (0.84)
I/σ (I)	38.3 (1.67)	34.9 (3.23)	41.9 (3.1)
Completeness (%)	99.1 (92.1)	98.7 (96.1)	99.5 (99.1)
Redundancy	13.1 (6.5)	13.3 (13.7)	7.0 (7.1)
Number of unique reflections	17072	13122	5681
R_{work}/R_{free} (%)	21.5/24.3	21.3/24.7	24.8/29.4
Number of nonhydrogen atoms			
Protein	1070	1035	948
Peptide	128	98	-
Water	122	47	7
Zn	8	8	8
Average B factors (Å^2)			
Protein	29.9	28.8	75.1
Peptide	38.6	35.6	-
Zn	34.3	25.3	76.9
Water	36.5	33.0	74.4
Rmsd			
Bond lengths (Å)	0.008	0.008	0.012
Bond angles (°)	1.167	1.115	1.700

[a] Highest-resolution shell (in Å) is shown in parentheses.

Crystal Structures of PHD$_{UHRF1}$ in Free and H3(1-9) Bound States

The above biochemical and molecular investigations raised the exciting possibility that PHD$_{UHRF1}$ may be an unmodified H3R2 "reader." To understand the molecular mechanism of PHD$_{UHRF1}$-mediated histone H3 recognition, we determined the crystal structures of PHD$_{UHRF1}$ in the free state and in complex with histone H3(1-9) and H3(1-9)K4me3 peptides, with crystallographic statistics listed in Table 1.

Canonical PHD fingers are defined by a cross-bracketed two Zn finger domain architecture (Aasland et al., 1995). Sequence comparison with canonical PHD fingers reveals that PHD$_{UHRF1}$ has an extra N-terminal motif containing three additional Cys residues when compared to the canonical sequence (see Figure S1A available online). Based on the 2.65 Å crystal structure of PHD$_{UHRF1}$ in the free state, the Pro311 to Val328 segment that is present N terminal to the canonical PHD finger adopts a knot-like fold designated the pre-PHD motif (cyan-colored fold in Figure S1B). Three Cys (315, 318, and 326) residues from the N-terminal Cys-rich pre-PHD motif and Cys329 from the N terminus of the canonical PHD finger coordinate a Zn ion (designated Zn1) to form the pre-PHD (Figure S1B), with a single helical turn connecting the pre-PHD and canonical PHD finger motifs, whose relative alignments are stabilized by hydrogen bonding interactions. Two symmetry-related monomers form a Zn-coordinated dimer for PHD$_{UHRF1}$ in the free state, mediated by a single Zn ion (designated Zn4) (Figure S1C).

We have solved the 1.80 Å structure of PHD$_{UHRF1}$ cocrystallized with unmodified H3(1-9) peptide. Two noncrystallographic symmetry-related monomers form a Zn-coordinated dimer for PHD$_{UHRF1}$ in the H3(1-9) bound state, mediated by a pair of Zn ions (designated Zn4) (Figure S1D). PHD$_{UHRF1}$ contacts the first four residues of the bound H3(1-9) peptide, with residue Arg8 interacting with a symmetry-related molecule. The A1-R2-T3-K4 residues of the bound H3 peptide are docked in an antiparallel alignment with the β1 strand on the surface of the PHD finger through peptide-protein backbone interactions (Figure 2A). The side chain of Ala1 of the bound peptide is buried within a pocket formed by hydrophobic residues Leu344, Pro366, and Trp371 (Figure 2A). In addition, the amino terminus of the peptide interacts with the main-chain carbonyl oxygen of Glu368 (Figure 2A).

The Arg2 side chain is docked on the negatively charged surface groove in the PHD finger (Figure 2B), with the Asp347-Asp350 hairpin segment that connects the β1 and β2 strands of the PHD finger playing a pivotal role in unmodified Arg2 recognition, through hydrogen bond formation of its NεH atom with the

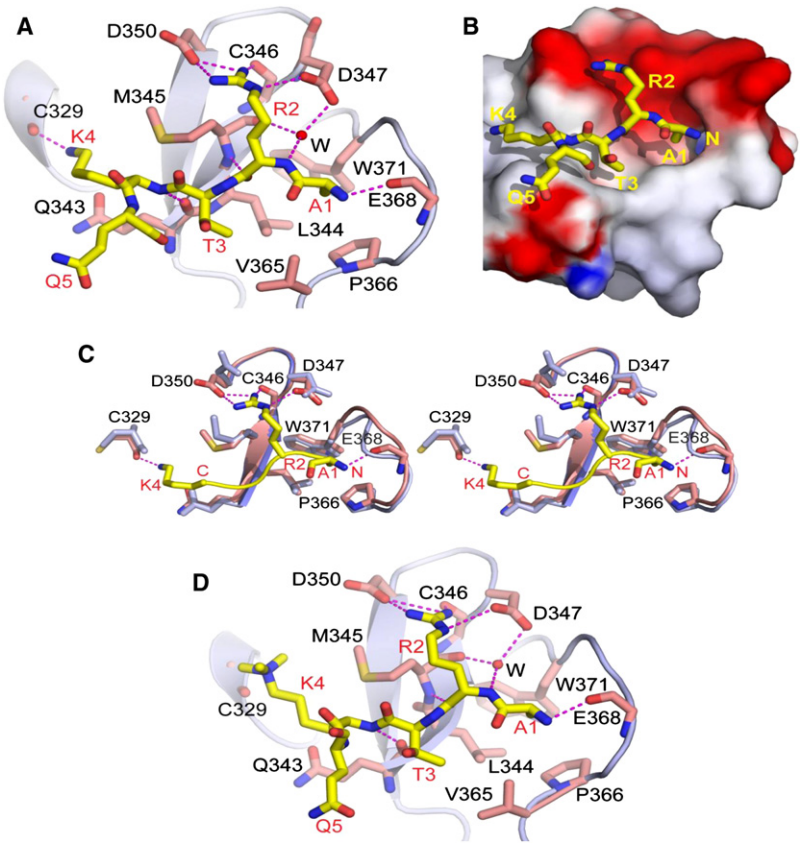

Figure 2. Crystal Structures of PHD_{UHRF1} Bound to H3(1-9) and H3(1-9)K4me3 Peptides

(A) Shown is a ribbon (protein) and stick (peptide) representation of the 1.80 Å crystal structure of PHD_{UHRF1} bound to H3(1-9) peptide. The PHD_{UHRF1} is colored in light blue, with the pre-PHD not shown in this view. The bound H3 peptide is colored in yellow, with interacting residues on PHD_{UHRF1} colored in magenta. Intermolecular interactions are depicted as magenta-colored dashed lines. A bridging water molecule involved in intermolecular recognition is shown as a red sphere.

(B) Shown is an electrostatic (protein) and stick (peptide) representation of the crystal structure of PHD_{UHRF1} bound to H3(1-9) peptide. The bound peptide is in yellow, and the side chain of R2 is positioned within the red-colored acidic surface patch of the protein.

(C) A stereo view of the superposition of the crystal structures of PHD_{UHRF1} in the free (light blue) and H3(1-9) peptide-bound (magenta) states. The H3(1-4) segment of the bound peptide is shown in yellow.

(D) A ribbon (protein) and stick (peptide) representation of the 1.95 Å crystal structure of PHD_{UHRF1} bound to H3(1-9) K4me3 peptide.

See also Figures S1 and S6.

side chain of Asp347 and both its $N\eta H_2$ atoms hydrogen bond with the side chain of Asp350 (Figure 2A). The backbone carbonyl oxygen of Cys346 also forms a polar contact with the $N\eta 2H$ proton of Arg2. In addition, an ordered water molecule mediates the network of hydrogen bond interactions such that it connects the backbone amide proton of Arg2 of the bound peptide with the main chain carbonyl oxygen of Met345 and the side chain of Asp347 of the protein (Figure 2A). Such an extensive array of hydrogen bonding interactions between Arg2 of the bound H3 peptide and the PHD finger provides an ample basis for the specificity of recognition of the unmodified H3R2 mark by PHD_{UHRF1}. Upon peptide binding, the Glu368-Glu370 segment is reorganized to accommodate the Ala1 residue at the N terminus of the peptide, and the Asp350 side chain undergoes a conformational change ($\chi 2$ angle changes from -19° to 23°) to facilitate H3 Arg2 side chain recognition (stereo view in Figure 2C comparing free [blue] and bound [magenta] structures).

The observed extensive network of intermolecular contacts involving Arg2 establishes that the PHD_{UHRF1} recognizes unmodified H3R2 in the structure of its complex (Figure 2A). This structural observation is supported by significant reduction in binding affinity between PHD_{UHRF1} and H3 peptides (Kd = 2.1 μM) when Arg2 is either symmetrically (Kd = 39.7 μM) or asymmetrically dimethylated (Kd = 44.9 μM) or substituted by Ala (Kd > 150 μM), while a smaller drop in binding affinity is observed on monomethyation of Arg2 (Kd = 7.6 μM) (Figure 3A).

Trimethylation at H3K9 by and large had no impact on binding (Kd = 2.5 μM), while trimethylation at H3K4 caused a modest reduction (Kd = 7.3 μM) (Figure 3B), consistent with the in vitro pull-down results with full-length UHRF1 (Figure 1B) and the 1.95 Å crystal structure of PHD_{UHRF1} bound to H3(1-9)K4me3 peptide (Figure 2D). Further, addition of an Ala-Ala segment at the N terminus of the H3 peptide results in a large drop in binding affinity (Kd > 400 μM) (Figure 3C), as did acetylation of the N terminus (Kd > 250 μM) (Figure 3C), highlighting the important contribution of the N terminus of H3 to PHD_{UHRF1} H3 recognition (Figure 2A). These findings, together with binding studies on the R2A mutant (Kd > 150 μM) (Figure 3A), lend further support to the notion that binding of PHD_{UHRF1} to H3 is mediated mainly by unmodified R2, supplemented by recognition of the N terminus of H3. Indeed, Asp347 and Asp350, which form hydrogen bonds with the guanidinium group of H3R2 in the complex (Figure 2A), when mutated to Ala, also result in a significant reduction in the binding affinities to Kd = 47.0 μM for the D350A mutant and Kd = 95.0 μM for the D347A mutant (Figure 3D).

Finally, PHD_{UHRF1} bound very weakly to histone H3 when T3 is phosphorylated (H3[1-15]T3ph) (Kd > 500 μM) (Figure 3C), indicative of complex destabilization from either steric and/or electrostatic repulsion following phosphorylation of T3 positioned adjacent to R2 in the H3 sequence.

PHD_{UHRF1} H3R2 Binding Is Critical for UHRF1-Regulated Gene Expression

The above biochemical and structural investigations revealed a protein modality that specifically recognizes unmodified R2 of H3, suggesting that this recognition may play an important role in directing UHRF1 to specific genomic locations. As

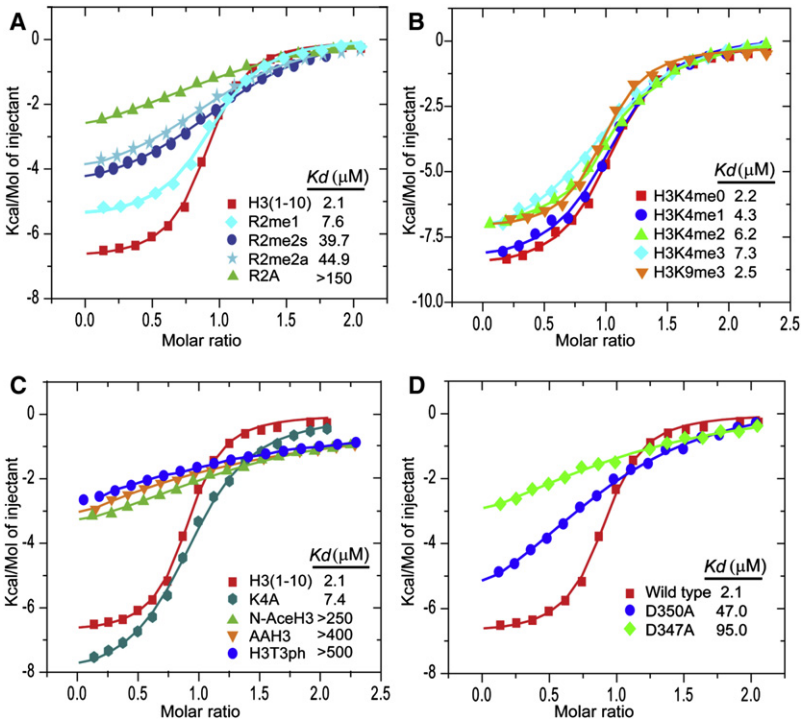

Figure 3. ITC Measurement of Interaction between PHD$_{UHRF1}$ and Histone H3 Tail

(A) Superposed exothermic ITC enthalpy plots for the binding of PHD$_{UHRF1}$ to H3(1-10), H3(1-10)R2me1, H3(1-10)R2me2s, H3(1-10)R2me2a, and H3(1-10)R2A peptides. The insert lists the measured binding constants.

(B) Superposed exothermic ITC enthalpy plots for the binding of PHD$_{UHRF1}$ to H3(1-15)K4me0, H3(1-15)K4me1, H3(1-15)K4me2, H3(1-15)K4me3, and H3(1-15)K9me3 peptides. The insert lists the measured binding constants.

(C) Superposed exothermic ITC enthalpy plots for the binding of PHD$_{UHRF1}$ to H3(1-10), H3(1-10)K4A, H3AA(1-10), N-acetyl H3(1-15), and H3(1-15)T3ph peptides. The insert lists the measured binding constants.

(D) Comparison of exothermic enthalpy plots for wild-type with D350A and D347A mutants of PHD$_{UHRF1}$ bound to H3(1-10) peptide.

discussed earlier, UHRF1 is found at PCH, but either deletion of PHD$_{UHRF1}$ or mutations of the H3R2-binding amino acids (D347A and adjacent E348A) showed PCH localization comparable to that of wild-type UHRF1 (Figure 4A), suggesting that H3R2 binding is likely to be dispensable for UHRF1 PCH localization. This is perhaps not unexpected, because UHRF1 PCH localization is believed to involve SRA$_{UHRF1}$, which binds hemi-methylated CpG (Bostick et al., 2007; Sharif et al., 2007), a hallmark modification of PCH (Richards and Elgin, 2002), although such a PCH-localizing role for SRA$_{UHRF1}$ has been questioned by a more recent study (Rottach et al., 2010). Collectively, our findings suggest that while PHD$_{UHRF1}$ appears dispensable for UHRF1 PCH localization, it could be critical for targeting UHRF1 to euchromatic locations.

To determine whether H3R2 binding is important for UHRF1 regulation of euchromatic gene expression, we carried out microarray analysis to identify UHRF1-regulated genes using RNAs isolated from cells treated with either scrambled or two independent UHRF1 shRNAs (uhrf1-sh2 and uhrf1-sh5). Each uhrf1 shRNA caused both up- and downregulation of approximately 3000 genes (Figure S2). However, genes that show expression changes in response to both uhrf1 shRNAs were in smaller numbers (367 and 606 up- and downregulated genes, respectively) (Table S1). We considered only those genes that show differential expression in cells treated with both UHRF1 shRNAs as potential UHRF1-regulated genes. Given that UHRF1 is primarily a repressor of transcription (Daskalos et al., 2011; Kim et al., 2009), we focused our initial validation efforts on those genes that were upregulated in the absence of UHRF1. RT-qPCR showed that out of the 26 genes, 22 were upregulated in the uhrf1 RNAi cells, representing greater than 80% confirmation rate (Figure 4B). GO term analysis identified potential involvement of UHRF1-regulated genes in RNA processing and metabolism, as well as cell death (Figures S3A and S3B), while KEGG Pathway analysis suggested possible regulation of cancer pathways by UHRF1 (Figure S3C), which are consistent with the previous reports of possible roles for UHRF1 in apoptosis and tumorigenesis (Abbady et al., 2003; Hervouet et al., 2010; Tien et al., 2011). Importantly, we demonstrated by ChIP followed by quantitative PCR (ChIP-qPCR) that these two UHRF1-regulated genes are bound by UHRF1 near promoters (Figure 4C), as well as gene bodies (data not shown), indicating that their expression is directly regulated by UHRF1. Consistently, ChIP also showed that the promoter regions of these two genes lack H3R2 methylation (H3R2me2s) (Figure 5A). These two promoters also lack H3K9 trimethylation (Figure 5B), which may explain the dependency on the PHD domain for UHRF1 regulation of these genes (see below). We also investigated DNA methylation status of these promoters and determined whether UHRF1 is involved in the regulation by methylated DNA immunoprecipitation (MeDIP) assays (Weber et al., 2007). As shown in Figure 5C, the 5-methyl-C antibodies (Eurogentec) detected MeDIP signals at the promoters of ADAM19 and SUSD2 as well as that of RARβ, which is known to be methylated (Widschwendter et al., 2000) (also Figure S4). Consistently, the MeDIP signals are significantly higher than that of RPL30, which is an actively transcribed gene and therefore is expected to have no or low levels of DNA methylation. Interestingly, knockdown of UHRF1 reduced methylation signals at both promoters (Figure 5C), suggesting that UHRF1-mediated repression of these two genes may involve DNA methylation. While insight into whether and how these UHRF1-regulated genes may play a role in mediating UHRF1 biology requires additional studies, these results nevertheless suggest that both histone and DNA methylation may play a role in UHRF1-regulated gene repression and provide UHRF1-regulated target genes for the genetic complementation experiments described below.

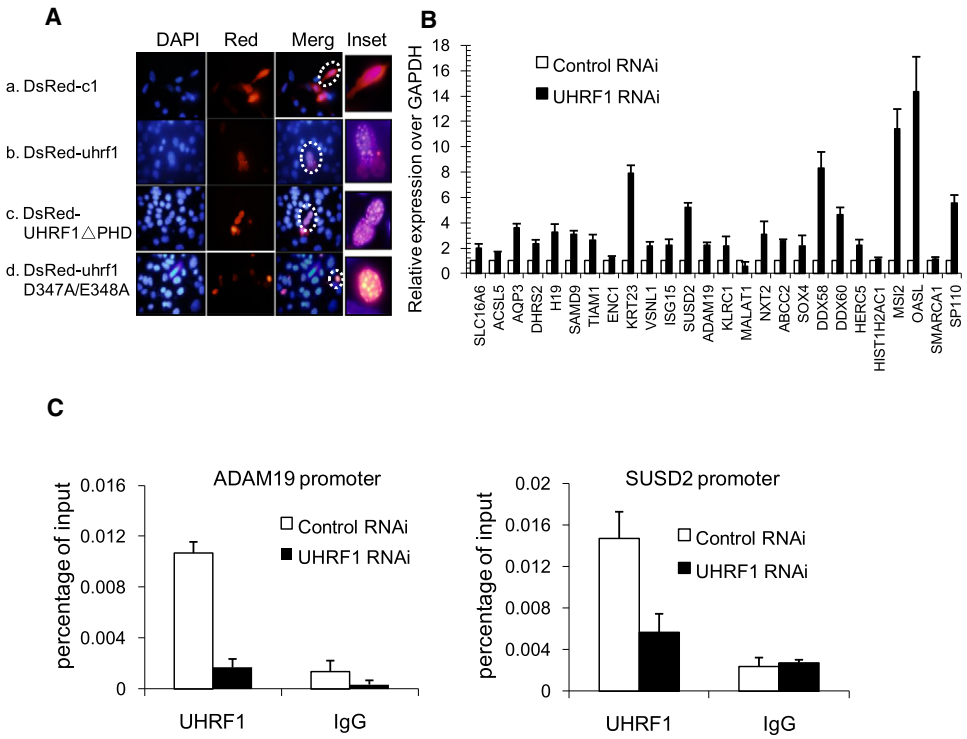

Figure 4. Identification of Target Genes Directly Regulated by UHRF1

(A) H3R2 binding is likely to be dispensable for UHRF1 PCH localization. dsRed-fused wild-type and mutant UHRF1 constructs were transfected into NIH 3T3 cells, and immunostaining was performed 2 days posttransfection. Representative cells were highlighted by dashed circles.

(B) Validation of microarray expression data with RT-qPCR. Twenty-six genes upregulated in our microarray were randomly selected for further validation. RNAs were prepared from plko.1-control shRNA and UHRF1-sh2-treated HCT116 cells and were reversed transcribed into cDNA for qRT-PCR. Error bars represent SEM calculated from three independent experiments.

(C) RNAi of UHRF1 results in decreased UHRF1 occupancy at its target genes (ADAM19 and SUSD2). Error bars represent SEM calculated from three independent experiments.

To determine the functional significance of PHD_{UHRF1} binding unmodified H3R2, we next carried out genetic complementation experiments using full-length, wild-type, and the R2-binding defective dual mutant (D347A and adjacent E348A), which showed undetectable H3 binding as determined by the ITC assay (Figure 6A). As shown in Figure 6B, wild-type, but not the binding-defective dual mutant of UHRF1 (D347A and adjacent E348A), restored repression of the two UHRF1-reguated genes, SUSD2 and ADAM19. Both the wild-type and the dual mutant proteins were comparably expressed, suggesting that the lack of rescue by the binding-defective mutant was not due to lack of expression (Figure S5). Taken together, these results suggest that the primary function of PHD_{UHRF1} is to localize UHRF1 to euchromatic targets by recognizing and binding the unmodified R2 residue.

DISCUSSION

Comparison of N-Terminal H3 Peptide Recognition by PHD_{UHRF1} and $WD40_{WDR5}$ Domains

In the present study, we have demonstrated that unmodified H3R2 recognition of PHD_{UHRF1}, mediated predominantly by inter-side-chain hydrogen bonds, represents a mode of histone H3 tail recognition. Recognition of unmodified H3R2 by its binding pocket within PHD_{UHRF1} involves both an electrostatic and hydrogen bonding contribution between its guanidinium group and the side chain of acidic residues (Figure 2B), as well as a hydrophobic contribution between its aliphatic side chain and the side chain of Met345 (Figure 2A). Indeed, dimethylation of Arg2, or its replacement by Ala, results in a pronounced drop in binding affinity (Figure 3A).

Previous studies identified the WD40 domain of WDR5, a component of the SET1/MLL family of histone methyltransferases, as a reader of unmodified H3R2 (Couture et al., 2006; Han et al., 2006; Ruthenburg et al., 2006; Schuetz et al., 2006). Recognition of unmodified H3R2 by $WD40_{WDR5}$ involves targeting of both the N terminus and insertion of the unmodified R2 side chain into the central cavity of the torroidal WD40 propeller fold, where it is oriented through direct and water-mediated hydrogen bonds and sandwiched between staggered Phe side chains (Figure S6B). However, there is an important distinction between the PHD_{UHRF1} (Figure S6A) and $WD40_{WDR5}$ (Figure S6B) complexes, since unmodified H3R2 is targeted by PHD_{UHRF1} using a "surface groove" recognition mode, whose binding pocket is more accessible, while it is targeted by $WD40_{WDR5}$ using a "cavity insertion" recognition mode, in which the mark

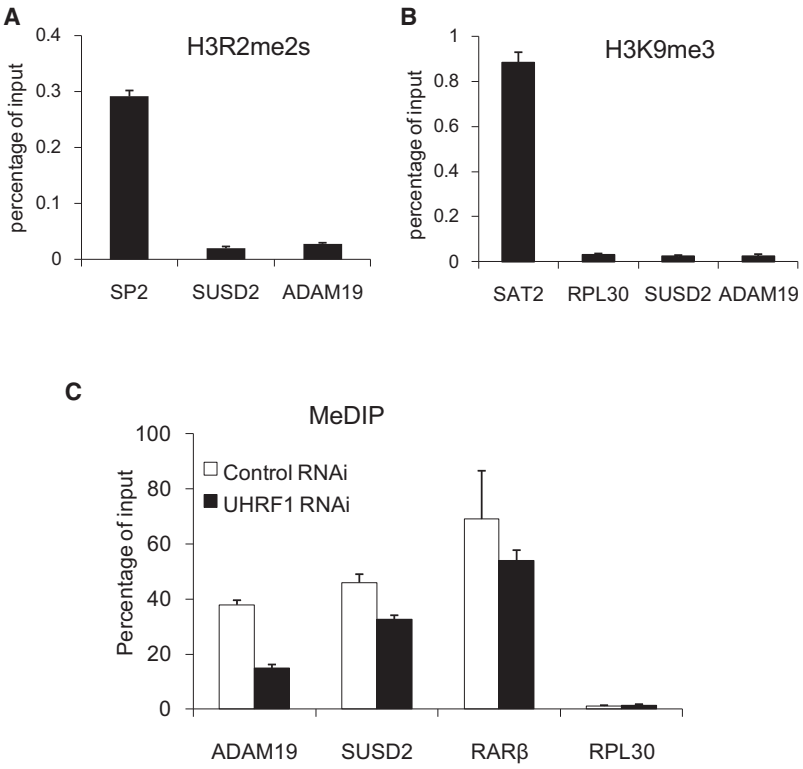

Figure 5. UHRF1 Direct Target Genes, ADAM19 and SUSD2, Lack H3R2me2s and H3K9me3 but Have DNA Cytosine Methylation at Their Promoters

(A) ADAM19 an SUSD2 promoters lack H3R2 symmetric dimethyation. H3R2me2s-specific polyclonal antibodies developed in the Guccione lab in Singapore were used for the ChIP experiments, and the Sp2 promoter was used as a positive control. Error bars represent SEM calculated from three independent experiments.

(B) UHRF1 direct targets are associated with low levels of H3K9me3. The same primers used in Figure 4C were used for H3K9me3 ChIP. The SAT2 repetitive sequence representing heterochromatic regions and the housekeeping gene RPL30 were used as positive and negative controls, respectively. Error bars represent SEM calculated from three independent experiments.

(C) ADAM19 and SUSD2 promoters are cytosine methylated, and methylation appears to require UHRF1. The 5-methyl-C antibodies were used for MeDIP analysis. MeDIP results were expressed as values relative to their corresponding input. RARβ and RPL30 were used as positive and negative controls, respectively. Error bars represent SD calculated from two independent experiments.

is inserted and buried within a deep protein cleft, with greater potential for size-selective discrimination (Taverna et al., 2007).

It should be noted that TUDOR$_{JMJD2A}$ (Huang et al., 2006; Lee et al., 2008) and ADD$_{DNMT3A}$ (Otani et al., 2009) that bind H3K4me3 and unmodified H3K4 marks, respectively, also display contacts with the unmodified H3R2 site. These TUDOR/ADD domains cannot be specified as readers of H3R2 marks since they do not form the extensive network of intermolecular hydrogen bonds to the guanidinium group of R2, as observed for the PHD$_{UHRF1}$ (Figure 2A). Further, much smaller reductions in binding affinities were observed following either methylation of R2 or its replacement by Ala for ADD$_{DNMT3A}$ and TUDOR$_{JMJD2A}$ compared to PHD$_{UHRF1}$.

Unlike other complexes involved in unmodified K4 recognition (Lan et al., 2007; Ooi et al., 2007), where the ammonium group forms multiple hydrogen bonds with acidic side chains, the side chain of unmodified H3K4 forms a single hydrogen bond to the backbone carbonyl of Cys329 in the PHD$_{UHRF1}$ complex

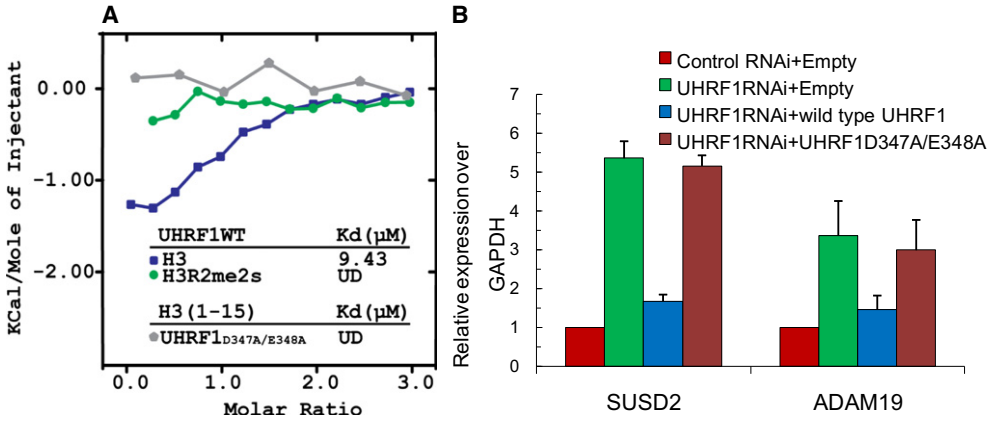

Figure 6. UHRF1 Binding H3R2 Is Critical for Its Ability to Regulate Target Gene Expression

(A) Superimposed ITC enthalpy plots for the binding of full-length UHRF1 (wild-type or mutant) and histone H3 peptides with the estimated binding affinity (Kd). UD, undetectable.

(B) Rescue experiments. RNAi-resistant wild-type UHRF1, but not the H3R2 binding-defective mutant of UHRF1 (D347A/E348A), restored repression of two UHRF1-reguated genes, SUSD2 and ADAM19, in UHRF1 RNAi cells. HCT116 stable cell lines were established that coexpress control or UHRF1 shRNA and/or indicated flag-tagged UHRF1 constructs. mRNA expression of SUSD2 and ADAM19 was measured by qPCR. GAPDH was used as an internal control. SEM was obtained from three independent experiments.

(Figure 2A and Figure S6A). Thus, there is ample room to accommodate methylation modifications at H3K4, as validated by binding studies as a function of K4 methylation state (Figure 3B) and the crystal structure of H3(1-9)K4me3 peptide bound to PHD_{UHRF1} (Figure 2D).

PHD_{UHRF1} Is Critical for Targeting UHRF1 to Euchromatic Locations and for Regulation of Euchromatic Gene Expression

UHRF1 has been shown to be mainly involved in heterochromatin function (Karagianni et al., 2008; Papait et al., 2008; Papait et al., 2007) and in CpG methylation regulation during DNA replication (Bostick et al., 2007; Sharif et al., 2007). Although previous studies identified a handful of genes regulated by UHRF1, suggesting a possible role for UHRF1 in gene expression regulation (Kim et al., 2009), our study investigated such a role for UHRF1 at the genome-wide level. Our analysis identified thousands of potential UHRF1 target genes, supporting a general transcriptional role for UHRF1. Earlier studies implicated UHRF1 in cell proliferation and apoptosis regulation (Fang et al., 2009; Fujimori et al., 1998; Tien et al., 2011) and suggested that UHRF1 may function as a possible oncogene (Bronner et al., 2007). Our GO term analysis (Figure S3) identified possible tumor suppressor genes such as Axin2 and BMP4, among UHRF1-upregulated genes, as well as genes in apoptosis, raising the exciting possibility that these genes may mediate UHRF1's ability to regulate cell proliferation and cell death. Interestingly, a number of previously reported, UHRF1-regulated genes involved in cancer such as BRCA1 and p73 are not among the UHRF1-regulated genes identified in our analysis. This could be due to cell type or assay condition differences. Regardless, our studies support the notion that UHRF1 directly regulates the expression of a large number of genes, setting the stage for future studies directed toward providing further insights into how these genes may mediate UHRF1 biology.

It is important to note that our findings have provided molecular and structural insights into how UHRF1 is targeted to euchromatic regions to exert its transcriptional roles, namely by recognizing and binding the unmodified H3R2 residue. We believe that the primary function of PHD_{UHRF1} is to target UHRF1 to euchromatic regions lacking H3K9me3. For those genes that carry H3K9me3, we predict that $Tudor_{UHRF1}$, which binds H3K9me3, will predominate and relieve the dependency on PHD_{UHRF1}. Consistent with this, we found that the presence of H3K9me3 counteracts the inhibitory effect of R2 dimethylation on UHRF1 binding to histone H3 in vitro (data not shown). In addition to the euchromatic targeting function of PHD_{UHRF1} reported here, previous studies also demonstrated the requirement of PHD_{UHRF1} in the regulation of PCH structure (Papait et al., 2008). Collectively, PHD_{UHRF1} appears to be important for targeting UHRF1 to euchromatic and for PCH function, although it is dispensable for PCH targeting.

Potential for Crosstalk between Histone Arginine Methylation and UHRF1 Function

In summary, we have provided binding, structural, and functional data highlighting the discovery of an effector module dedicated to the recognition of an unmodified arginine residue (R2) on histone H3. Our findings further suggest that any modifications of R2 may negatively impact on UHRF1 binding to H3, including methylation (Figures 2 and 3) and possibly deimination (Cuthbert et al., 2004), raising the possibility of crosstalk between UHRF1 chromatin binding and pathways that regulate H3R2 posttranslational modifications. Interestingly, R2 monomethylation exhibits a lesser impact on UHRF1 H3 binding (3.5-fold reduction, Figure 3A) compared to symmetrical and asymmetrical dimethylation (20-fold reduction in binding, Figure 3A), suggesting that subtle differences in R2 modifications may impart differential regulation on UHRF1 chromatin binding. The potential functional significance of mono- versus dimethylation of UHRF1 regulation remains unclear and awaits a better understanding of the methyltransferases involved in these modifications. Together with recent reports of readout of methylated arginine marks on histone (Yang et al., 2010) and protein (Liu et al., 2010a, 2010b) by TUDOR domains, these findings begin to uncover a potentially elaborate effector network for the recognition of differential methylation states on histone arginine residues.

EXPERIMENTAL PROCEDURES

Protein Expression and Purification

All constructs were generated using PCR-based cloning strategy, and all mutants were generated by the QuikChange Mutagenesis protocol (Stratagene). DNA fragments of full-length UHRF1 (1–806), Tudor (139–298), and PHD (311–379) were subcloned into pGEX-6P-1 or pET-15b derivative encoding a 3C protease cleavage site. All constructs were expressed in *Escherichia coli* strain BL21(DE3) and purified using glutathione 4B column chromatography. The PHD finger (311–380), as well as TUDOR (140–295) and SRA (427–630), were also cloned into GST- and hexahistidine-sumo-tagged expression vectors, respectively. The expression conditions and sequential protein purification protocols are detailed in the Supplemental Experimental Procedures.

Peptide Pull-Down Assays

Biotinylated histone peptides (1 μg each) were used for the pull-down assays with either GST-fused PHD or his6-tagged full-length UHRF1 following the binding protocol described previously (Lan et al., 2007).

Antibodies

UHRF1 polyclonal antibodies were raised in house, while H3R2me2s antibodies were rabbit polyconal antibodies produced and quality controlled in the Gucioone lab in Singapore (eguccione@imcb.a-star.edu.sg).

ITC Measurements

Isothermal titration calorimetric experiments were performed using a VP-ITC calorimeter (MicroCal, LLC) at 25°C with MicroCal Origin software used for curve fitting, equilibrium dissociation constant, and molar ratio calculations. For detailed procedures, see the Supplemental Experimental Procedures.

Crystallization, X-Ray Data Collection, and Structure Determination

Crystallization trials of PHD_{UHRF1} bound to unmodified and methylated N-terminal H3 peptides were conducted at 18°C by the sitting drop vapor diffusion method using a MOSQUITO crystallization robot. The X-ray data set on crystals of PHD_{UHRF1} in free state, and bound to variants of H3 peptide, was collected at the beam lines mentioned in Table 1. The crystal structure of the complex of PHD_{UHRF1} bound to H3(1-9) was solved by single-wavelength anomalous dispersion (SAD) technique at Zn-peak wavelength. Subsequent structures of PHD_{UHRF1} and its complexes were solved by molecular replacement method using the structure of the PHD_{UHRF1} bound to H3(1-9) as a search model.

Additional details related to crystallization, data collection, and structure calculations are provided in the Supplemental Experimental Procedures. The crystallographic statistics for all structures presented above are listed in Table 1.

RNA Interference and Genetic Rescue

Lentiviral Plko.1 constructs expressing shRNAs (sequences listed in Table S2) were purchased from Open Biosystems. Viral particles were produced in 293T cells by following the recommended protocols (Addgene). Stable HCT116 cell lines were established with coexpressed Lentiviral plenti6.2, or plenti6.2-UHRF1 (wild-type or mutant) and plko.1 shRNAs (control or UHRF1 RNAi). Twenty-four hours after infection, puromycin and Blasticidin S hydrochloride were added at 1.6 μg/ml and 5 μg/ml, respectively, to select for pooled populations of stably infected cells. Cells were then harvested for RNA extraction after 6 days' selection. Reverse transcription was performed with 1 μg RNA followed by real-time PCR. The primers for real-time PCR are listed in Table S3.

Gene Expression Microarray Analysis

Microarray analysis for global gene expression was performed using standard methods on the Affymetrix GeneChip System.

Methylated DNA Immunoprecipitation

After treatment with UHRF1shRNA and contol lentivirus for 14 days, genomic DNA was purified from HCT116 cells, sonicated, denatured, and incubated (8 μg) with a monoclonal antibody against 5-methyl-C (Eurogentec) (10 μl) at 4°C for 4 hr. The antibody-DNA complexes were captured by protein A/G beads, and the DNA enrichments in the MeDIP fraction were measured by real-time PCR.

ACCESSION NUMBERS

The atomic coordinates and structure factors have been deposited in the Protein Data Bank with the following accession codes: PHD$_{UHRF1}$ in the free state (3SOX), complex with H3(1-9) peptide (3SOU), and complex with bound H3(1-9)K4me3 peptide (3SOW). The UHRF1 microarray data have been deposited in the GEO database under the accession number GSE30478.

SUPPLEMENTAL INFORMATION

Supplemental Information includes six figures, three tables, Supplemental Experimental Procedures, and Supplemental References and can be found with this article online at doi:10.1016/j.molcel.2011.07.006.

ACKNOWLEDGMENTS

We thank Yang Xiang, Degui Chen, and members of the Epigenetics Laboratory at Institutes of Biomedical Sciences, Fudan University, as well as Steve Jacobson and Greg Horowitz of UCLA Medical School and Mary Goll of the Memorial Sloan-Kettering Cancer Center for their interest and for helpful discussions. We thank Ernesto Guccione for the H3R2me2s antibodies and primers for Sp2 and Or Gozani for histone peptides. We thank the staff at beamlines 24ID-C and 24ID-E of the Advanced Photon Source at the Argonne National Laboratory, as well as the staff at BNL X29 of the Brookhaven National Laboratory for assistance with X-ray data collection. This work was supported by the Starr Foundation and a Leukemia-Lymphoma Program Project Grant (D.J.P) and by the "985" Program from the Chinese Ministry of Education and "973" State Key Development Program of Basic Research of China (2009CB825602, 2009CB825603) to the Epigenetics Laboratory at the Institute of Biomedical Sciences, Fudan University, Shanghai, China. Author contributions are as follows. E.R. was responsible for the ITC, crystallization, crystallographic data collection, and structure analysis, with assistance from H.L., under the supervision of D.J.P. The binding, genetic rescue, expression microarry analysis, cellular location of UHRF1 (wild-type and mutant), MeDIP, and ChIP experiments were undertaken by Z.W., H.M., and L.H. (under the supervision of F.L., Y.G.S., Y.X., and Y.S.). Y.L did the ITC experiment shown in Figure 6, and H.C. participated in the construction of various plasmids used in this study. R.G. and F.W. made technical and bioinformatics contributions, respectively. This manuscript was written by Y.S. and D.J.P. with input from the other authors. F.L. is an employee of Constellation Pharmaceuticals, Inc. Y.S. is a cofounder of Constellation Pharmaceuticals, Inc., and a member of its scientific advisory board.

Received: May 9, 2011
Revised: July 6, 2011
Accepted: July 7, 2011
Published: July 21, 2011

REFERENCES

Aasland, R., Gibson, T.J., and Stewart, A.F. (1995). The Phd finger—implications for chromatin-mediated transcriptional regulation. Trends Biochem. Sci. *20*, 56–59.

Abbady, A.Q., Bronner, C., Trotzier, M.A., Hopfner, R., Bathami, K., Muller, C.D., Jeanblanc, M., and Mousli, M. (2003). ICBP90 expression is downregulated in apoptosis-induced Jurkat cells. Ann. N Y Acad. Sci. *1010*, 300–303.

Bedford, M., and Clark, S.G. (2009). Protein arginine methylation in mammals: who, what, and why. Mol. Cell *33*, 1–13.

Bostick, M., Kim, J.K., Esteve, P.O., Clark, A., Pradhan, S., and Jacobsen, S.E. (2007). UHRF1 plays a role in maintaining DNA methylation in mammalian cells. Science *317*, 1760–1764.

Bronner, C., Achour, M., Arima, Y., Chataigneau, T., Saya, H., and Schini-Kerth, V.B. (2007). The UHRF family: oncogenes that are drugable targets for cancer therapy in the near future? Pharmacol. Ther. *115*, 419–434.

Citterio, E., Papait, R., Nicassio, F., Vecchi, M., Gomiero, P., Mantovani, R., Di Fiore, P.P., and Bonapace, I.M. (2004). Np95 is a histone-binding protein endowed with ubiquitin ligase activity. Mol. Cell. Biol. *24*, 2526–2535.

Couture, J.F., Collazo, E., and Trievel, R.C. (2006). Molecular recognition of histone H3 by the WD40 protein WDR5. Nat. Struct. Mol. Biol. *13*, 698–703.

Cuthbert, G.L., Daujat, S., Snowden, A.W., Erdjument-Bromage, H., Hagiwara, T., Yamada, M., Schneider, R., Gregory, P.D., Tempst, P., Bannister, A.J., et al. (2004). Histone deimination antagonizes arginine methylation. Cell *118*, 545–553.

Daskalos, A., Oleksiewicz, U., Filia, A., Nikolaidis, G., Xinarianos, G., Gosney, J.R., Malliri, A., Field, J.K., and Liloglou, T. (2011). UHRF1-mediated tumor suppressor gene inactivation in nonsmall cell lung cancer. Cancer *117*, 1027–1037.

Fang, Z.Y., Xing, F.Y., Bronner, C., Teng, Z.P., and Guo, Z.F. (2009). ICBP90 mediates the ERK1/2 signaling to regulate the proliferation of Jurkat T cells. Cell. Immunol. *257*, 80–87.

Fujimori, A., Matsuda, Y., Takemoto, Y., Hashimoto, Y., Kubo, E., Araki, R., Fukumura, R., Mita, K., Tatsumi, K., and Muto, M. (1998). Cloning and mapping of Np95 gene which encodes a novel nuclear protein associated with cell proliferation. Mamm. Genome *9*, 1032–1035.

Han, Z.F., Guo, L., Wang, H.Y., Shen, Y., Deng, X.W., and Chai, J.J. (2006). Structural basis for the specific recognition of methylated histone H3 lysine 4 by the WD-40 protein WDR5. Mol. Cell *22*, 137–144.

Hervouet, E., Lalier, L., Debien, E., Cheray, M., Geairon, A., Rogniaux, H., Loussouarn, D., Martin, S.A., Vallette, F.M., and Cartron, P.F. (2010). Disruption of Dnmt1/PCNA/UHRF1 interactions promotes tumorigenesis from human and mice glial cells. PLoS ONE *5*, e11333. 10.1371/journal.pone.0011333.

Huang, Y., Fang, J., Bedford, M.T., Zhang, Y., and Xu, R.M. (2006). Recognition of histone H3 lysine-4 methylation by the double tudor domain of JMJD2A. Science *312*, 748–751.

Karagianni, P., Amazit, L., Qin, J., and Wong, J. (2008). ICBP90, a novel methyl K9 H3 binding protein linking protein ubiquitination with heterochromatin formation. Mol. Cell. Biol. *28*, 705–717.

Kim, J.K., Esteve, P.O., Jacobsen, S.E., and Pradhan, S. (2009). UHRF1 binds G9a and participates in p21 transcriptional regulation in mammalian cells. Nucleic Acids Res. *37*, 493–505.

Lan, F., Collins, R.E., De Cegli, R., Alpatov, R., Horton, J.R., Shi, X., Gozani, O., Cheng, X., and Shi, Y. (2007). Recognition of unmethylated histone H3 lysine 4 links BHC80 to LSD1-mediated gene repression. Nature *448*, 718–722.

Lee, J., Thompson, J.R., Botuyan, M.V., and Mer, G. (2008). Distinct binding modes specify the recognition of methylated histones H3K4 and H4K20 by JMJD2A tudor. Nat. Struct. Mol. Biol. *15*, 109–111.

Liu, H., Wang, J.Y., Huang, Y., Li, Z., Gong, W., Lehmann, R., and Xu, R.M. (2010a). Structural basis for methylarginine-dependent recognition of Aubergine by Tudor. Genes Dev. *24*, 1876–1881.

Liu, K., Chen, C., Guo, Y., Lam, R., Bian, C., Xu, C., Zhao, D.Y., Jin, J., MacKenzie, F., Pawson, T., et al. (2010b). Structural basis for recognition of arginine methylated Piwi proteins by the extended Tudor domain. Proc. Natl. Acad. Sci. USA *107*, 18398–18403.

Ooi, S.K., Qiu, C., Bernstein, E., Li, K., Jia, D., Yang, Z., Erdjument-Bromage, H., Tempst, P., Lin, S.P., Allis, C.D., et al. (2007). DNMT3L connects unmethylated lysine 4 of histone H3 to de novo methylation of DNA. Nature *448*, 714–717.

Otani, J., Nankumo, T., Arita, K., Ikamoto, S., Ariyoshi, M., and Shirakawa, M. (2009). Structural basis for recognition of H3K4 methylation status by the DNA methyltransferase 3A ATRX-DNMT3-DNMT3L domain. EMBO Rep. *10*, 1235–1241.

Papait, R., Pistore, C., Negri, D., Pecoraro, D., Cantarini, L., and Bonapace, I.M. (2007). Np95 is implicated in pericentromeric heterochromatin replication and in major satellite silencing. Mol. Biol. Cell *18*, 1098–1106.

Papait, R., Pistore, C., Grazini, U., Babbio, F., Cogliati, S., Pecoraro, D., Brino, L., Morand, A.L., Dechampesme, A.M., Spada, F., et al. (2008). The PHD domain of Np95 (mUHRF1) is involved in large-scale reorganization of pericentromeric heterochromatin. Mol. Biol. Cell *19*, 3554–3563.

Richards, E.J., and Elgin, S.C. (2002). Epigenetic codes for heterochromatin formation and silencing: rounding up the usual suspects. Cell *108*, 489–500.

Rottach, A., Frauer, C., Pichler, G., Bonapace, I.M., Spada, F., and Leonhardt, H. (2010). The multi-domain protein Np95 connects DNA methylation and histone modification. Nucleic Acids Res. *38*, 1796–1804.

Ruthenburg, A.J., Wang, W.K., Graybosch, D.M., Li, H.T., Allis, C.D., Patel, D.J., and Verdine, G.L. (2006). Histone H3 recognition and presentation by the WDR5 module of the MLL1 complex. Nat. Struct. Mol. Biol. *13*, 704–712.

Schuetz, A., Allali-Hassani, A., Martin, F., Loppnau, P., Vedadi, M., Bochkarev, A., Plotnikov, A.N., Arrowsmith, C.H., and Min, J.R. (2006). Structural basis for molecular recognition and presentation of histone H3 By WDR5. EMBO J. *25*, 4245–4252.

Sharif, J., Muto, M., Takebayashi, S.I., Suetake, I., Iwamatsu, A., Endo, T.A., Shinga, J., Mizutani-Koseki, Y., Toyoda, T., Okamura, K., et al. (2007). The SRA protein Np95 mediates epigenetic inheritance by recruiting Dnmt1 to methylated DNA. Nature *450*, 908–925.

Shi, X., Hong, T., Walter, K.L., Ewalt, M., Michishita, E., Hung, T., Carney, D., Pena, P., Lan, F., Kaadige, M.R., et al. (2006). ING2 PHD domain links histone H3 lysine 4 methylation to active gene repression. Nature *442*, 96–99.

Taverna, S.D., Li, H., Ruthenburg, A.J., Allis, C.D., and Patel, D.J. (2007). How chromatin-binding modules interpret histone modifications: lessons from professional pocket pickers. Nat. Struct. Mol. Biol. *14*, 1025–1040.

Tien, A.L., Senbanerjee, S., Kulkarni, A., Mudbhary, R., Goudreau, B., Ganesan, S., Sadler, K.C., and Ukomadu, C. (2011). UHRF1 depletion causes a G2/M arrest, activation of DNA damage response and apoptosis. Biochem. J. *435*, 175–185.

Walker, A.G., Jr., Xue, S., Dong, A., Li, Y., Bountra, C., Weigelt, J., Arrowsmith, C.H., Edwards, A.M., Bochkarev, A., and Dhe-Paganon, S. (2008). Cryptic tandem tudor domains in UHRF1 interact with H3K9ME and are important for pericentric heterochromatin replication. http://www.rcsb.org/pdb/3DB3.PDB.

Weber, M., Hellmann, I., Stadler, M.B., Ramos, L., Paabo, S., Rebhan, M., and Schubeler, D. (2007). Distribution, silencing potential and evolutionary impact of promoter DNA methylation in the human genome. Nat. Genet. *39*, 457–466.

Widschwendter, M., Berger, J., Hermann, M., Muller, H.M., Amberger, A., Zeschnigk, M., Widschwendter, A., Abendstein, B., Zeimet, A.G., Daxenbichler, G., et al. (2000). Methylation and silencing of the retinoic acid receptor-beta2 gene in breast cancer. J. Natl. Cancer Inst. *92*, 826–832.

Yang, Y.Z., Lu, Y., Espejo, A., Wu, J.C., Xu, W., Liang, S.D., and Bedford, M.T. (2010). TDRD3 is an effector molecule for arginine-methylated histone marks. Mol. Cell *40*, 1016–1023.